Res Chem Intermed (2017) 43:5829–5839
DOI 10.1007/s11164-017-2965-9

Pt–NiO–Al_2O_3/G derived from graphene-supported layered double hydroxide as efficient catalyst for *p*-nitrophenol reduction

Elham Akbarzadeh[1] · **Mohammad Reza Gholami**[1]

Received: 14 February 2017 / Accepted: 18 April 2017 / Published online: 28 April 2017

Abstract The present work reports the synthesis of a Pt-modified NiO–Al_2O_3 nanocomposite derived from graphene-supported layered double hydroxide (Pt–NiO/G) and demonstrates its catalytic activity. The resulting Pt–NiO/G nanocomposite was characterized by FT-IR, XRD, FE-SEM, TEM and XPS techniques and used for catalytic reduction of *p*-nitrophenol (P-NP) to *p*-aminophenol (P-AP). The influence of graphene on catalytic activity was comparatively considered by preparation of Pt–NiO nanoparticles derived from layered double hydroxide. The superior catalytic performance of Pt–NiO/G was ascribed to the synergistic effect between Pt and NiO. Furthermore, reduction of P-NP was considered to follow a pseudo-first-order kinetic and a Langmuir–Hinshelwood model was suggested for the mechanism of reduction reaction.

Keywords Nickel oxide · Layered double hydroxide · *p*-nitrophenol · Reduction · Langmuir–Hinshelwood model

Introduction

p-Nitrophenol (P-NP) is one of the most rampant refractory pollutants in industrial wastewaters, while *p*-aminophenol (P-AP) is an important intermediate for the synthesis of pharmaceuticals, polymers, acetanilide and dyestuff [1–3]. P-AP can be produced by hydrogenation of P-NP using stoichiometric or excess amounts of reducing agents such as $NaBH_4$. However, reduction of P-NP by $NaBH_4$ is thermodynamically prosperous, and this reaction cannot progress efficiently without

✉ Mohammad Reza Gholami
gholami@sharif.edu

[1] Department of Chemistry, Sharif University of Technology, Tehran 11365-11155, Iran

a catalyst [4–6]. Hence, researchers have explored various materials as the catalyst for acceleration of this reaction.

Although the most significant catalysts that have been investigated for the reduction of P-NP are metal nanoparticles [7–10], there are several reports about using metal oxides as the catalyst for this reaction [11–15]. However, metal oxides show lower catalytic activity than precious metal nanoparticles and more research is needed to improve their catalytic properties for reduction reactions. In this regard, surface modification of metal oxides by active metal nanoparticles can be an ideal strategy to enhance the performance of these catalysts.

Using well-dispersed noble metals on layered double hydroxides (LDHs) surface is a facile technique to achieve highly active catalysts [16–18]. LDHs have been demonstrated by the common formula $([M^{2+}_{1-x}M^{3+}_{x}\ (OH)_2]^{x+}(A^{n-})_{x/n}\cdot mH_2O)$ to belong to a category of layered materials composed of metal hydroxide layers with a positive charge and anions in the interlayer space as the charge-compensating factor [19]. Extensive flexibility of the types of divalent (M^{2+}) and trivalent metal (M^{3+}) cations is an additional benefit receiving increasing interest in the use of these materials as a precursor for the synthesis of many metal oxide systems [20, 21].

Graphene has been widely used as a support for catalyst particles due to its fascinating properties such as remarkable thermal and chemical stability, high specific surface area and high conductivity. Graphene has been applied as the support for LDHs in several previous works and its full benefits in increasing the surface area and avoiding agglomerations have been reported [22, 23].

The present study aims to investigate NiO as a catalyst for P-NP reduction, and the effect of Pt as cocatalyst and graphene as support on its catalytic activity. NiO has been studied as an efficient catalyst and photocatalyst in several works [24, 25]; however, there are a few reports of its application for P-NP reduction [26]. On the other hand, NiAl-LDH is an ideal precursor for the synthesis of very well dispersed NiO particles [27, 28] In the present work, we synthesized graphene-supported Pt–NiO–Al_2O_3 NPs (Pt–NiO/G) derived from a NiAl-LDH precursor (Scheme 1). Also, the effects of graphene and Pt on the catalytic activity of NiO were investigated in a P-NP reduction reaction.

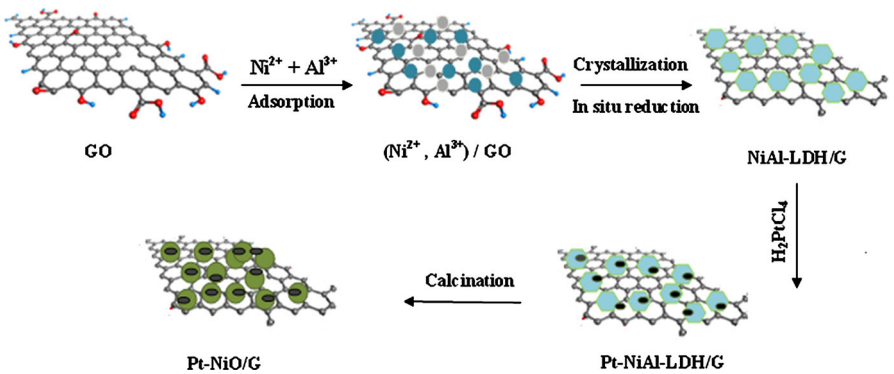

Scheme 1 Schematic diagram of synthetic process of Pt–NiO/G

Experimental

Synthesis of NiAl-LDH/G

GO was produced from natural graphite by a modified Hummers method [29]. For the preparation of NiAl-LDH, first, an aqueous solution of the precursors, Ni$(NO_3)\cdot 6H_2O$ (3 mmol) and Al$(NO_3)\cdot 7H_2O$ (1 mmol), was dispersed in GO suspension and ultrasonicated for 1 h. Then, the pH of the reaction was raised to 9.0 by drop-by-drop addition of an alkali solution of NaOH and Na_2CO_3 under vigorous stirring. The final suspension was transferred into a 100-mL Teflon-lined stainless steel autoclave and maintained 95 °C for 12 h. The resulting powder was collected and washed with deionized water several times until pH = 7.0, and then dried at 60 °C for 24 h. NiAl-LDH was synthesized under the same conditions without GO.

Synthesis of Pt–NiAl-LDH/G

To prepare Pt–NiAl-LDH/GO, first, a suspension of NiAl-LDH/G was prepared by dispersion of a certain amount as the synthesized precursor in deionized water under ultrasonication. Then, 0.4 mL H_2PtCl_6 solution (0.02 M) and 0.1 g urea were added to the solution under vigorous stirring, and the resulting suspension was stirred for 8 h at 90 °C. The composite was separated and washed with deionized water for several times until pH = 7.0. Pt–NiAl-LDH was synthesized under the same conditions.

Synthesis of Pt–NiO/G

After drying at 60 °C, the as-obtained powders were calcined in a tube-furnace reactor under N_2 flow, while the temperature of the furnace was increased from 25 to 600 °C at a rate of 5 °C min^{-1} and kept at 600 °C for 2 h. After cooling to room temperature, calcined Pt–NiAl-LDH/G was marked as Pt–NiO/G. Based on the ICP analysis, the content of Pt in the composite was determined to be 2.3 wt%. For comparison, pure NiAl-LDH/G and Pt–NiAl-LDH were calcined under the same conditions and were called NiO/G and Pt–NiO.

Characterization

An ABB BOMER MB series spectrophotometer was used to obtain the Fourier-transform infrared (FT-IR) spectra. A Philips X'pert instrument with a Cu Kα irradiation ($\lambda = 0.15418$ nm) at 40 kV/40 mA was used to record the crystalline structure of the samples. Hitachi S-4160 field emission scanning electron microscopy (FESEM) and a Philips CM30 150-kV transition electron microscopy (TEM) analyses were applied to observe the morphologies and particle distribution of the prepared catalyst. An X-ray photoelectron spectroscopy (XPS) equipped with

an Al–Kα X-ray source at an energy of 1486.6 eV was used to further analyze the surface composition and metal oxidation state of the Pt–NiO/G nanocomposite.

Catalytic reduction of p-nitrophenol

To examine the catalytic activity of the as-prepared nanocomposite, reduction of *p*-nitrophenol to *p*-aminophenol in the presence of $NaBH_4$ was chosen as an example reaction. At the first step, 0.1 mL (0.1 M) of freshly prepared $NaBH_4$ solution was added to 3 mL (0.1 mM) aqueous solution of P-NA. After addition of $NaBH_4$ solution, the P-NP solution exhibited a bright yellow color due to the formation of *p*-nitrophenolate ions. Next, 1 mg of catalyst was added to the above solution and the reduction reaction was started. The reaction progress was monitored by recording the intensity of the absorption peak of the *p*-nitrophenolate ions at 400 nm by UV–Vis spectra at certain interval times.

Results and discussion

Figure 1 indicates the FT-IR spectra of LDH/G (a), calcined LHD/G (b), and Pt–NiO/G (c). In the LDH/G spectrum, two bands at 1354 and 867 cm^{-1} correspond to the ϑ_3 and ϑ_2 vibration of CO_3^{-2}, respectively, which signify the existence of CO_3^{-2} anions in the LDH phase [30]. The bands that are visible at low frequency are assigned to the metal–O vibration mode in the LDH layers. As can be seen in the calcined LDH/G spectrum, the layered structure is diminished and the intense peak

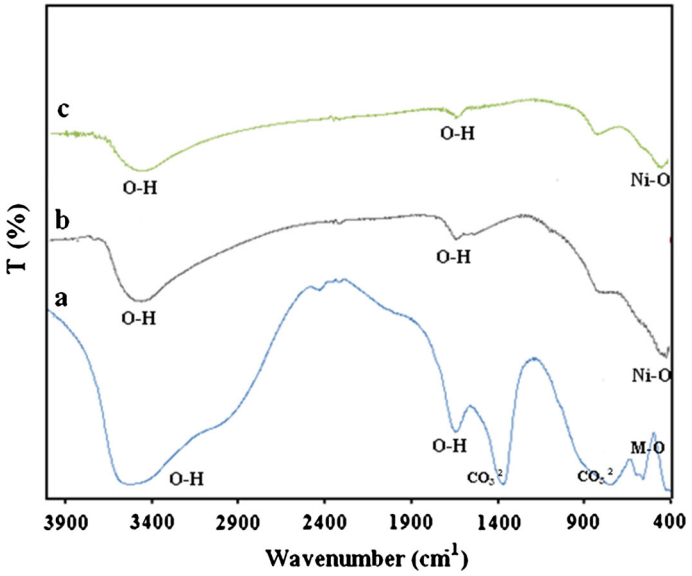

Fig. 1 FT-IR spectra of LDH/GO (**a**), calcined LHD/G (**b**) and Pt–NiO/G (**c**)

appearing at around 425 cm^{-1} represents the Ni–O band [31]. In Pt–NiO/G, the Ni–O band is visible, and any additional characteristic peak is not observable.

Figure 2 shows the XRD patterns of LDH/G, calcined LHD/G and Pt-NiO/G. LDH-G indicates distinct diffraction peaks at 2θ values of 11.5, 23, 34.9, 39, 46, 60.9 and 62.2 which demonstrate that the LDH-phase has been formed in the sample [32]. However, no obvious characteristic peak of G can be attributed to its very low content in the precursor. It is obvious that, after thermal treatment, the XRD patterns of the calcined materials illustrate three characteristic peaks at 2θ values of 37, 43 and 63, which are matched with the (111), (200) and (220) planes of the standard spectra of cthe ubic phase of NiO (JCPDS 04-0835) [33]. No diffraction peaks corresponding to the Al_2O_3 phase can be perceived, implying that the amorphous form of Al_2O_3 in the composite results from calcinations of the Al-containing LDHs [22]. However, the absence of the characteristic peaks of Pt^0 on the well-distributed atoms among the catalysts emphasize that they could not be identified by XRD [18].

The morphology of the Pt–NiO/G nanocatalyst was investigated by FESEM and TEM techniques. It is obvious from the SEM (a) and TEM images (b and c) that nano-sized Pt–NiO were densely distributed on the surface of the graphene sheets (Fig. 3a, b). Figure 3c indicates a magnified TEM image of the nanocomposite. As can be seen, the Pt nanoparticles were sporadically dispensed on the calcined LDHs surface which verifies that the Pt–NiO/G composite was successfully synthesized.

In order to analyze the surface composition and metal oxidation state, XPS characterization of Pt–NiO/G was performed. The survey spectrum of the Pt–NiO/G composite Fig. 5a exhibits the elemental composition of the surface, in which the peaks of Ni 2*p* and Pt 4*f* can be obviously seen. The high-resolution XPS spectrum of Ni 2*p* verifies that the valance state of element Ni is +2 (Fig. 4b). In addition, the Pt 4*f* spectrum of Pt–NiO/G contains two peaks corresponding to Pt $4f_{5/2}$ and Pt $4f_{7/2}$, which verifies that the platinum mainly exists in the metallic form (Fig. 4c).

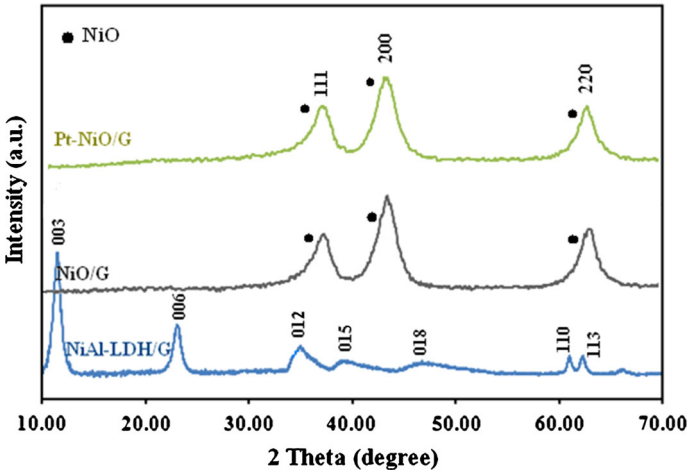

Fig. 2 XRD patterns of LDH/GO (**a**), calcined LHD/G (**b**) and Pt–NiO/G (**c**)

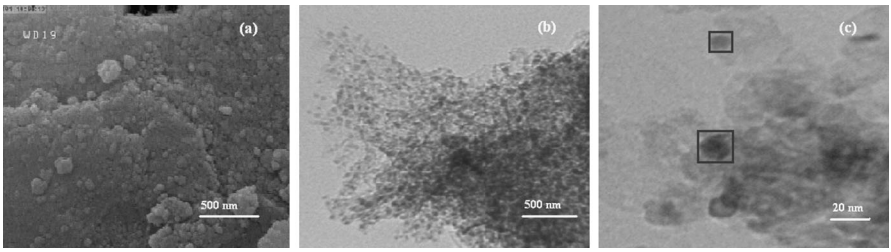

Fig. 3 SEM (**a**) and TEM images of Pt–NiO/G (**b**, **c**)

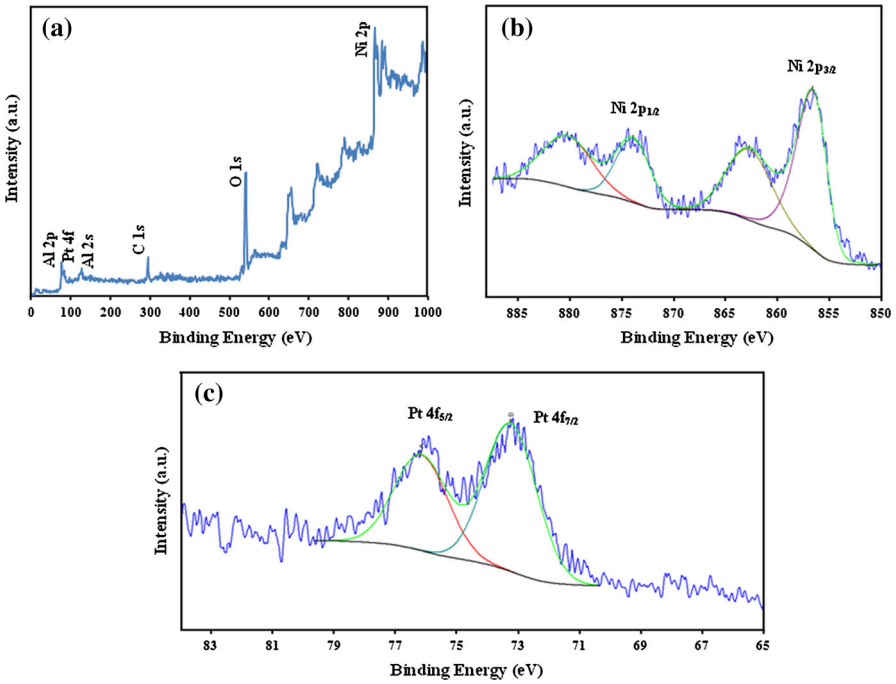

Fig. 4 XPS survey (**a**), Ni 2*p* (**b**) and Pt 4*f* (**c**) spectra of Pt–NiO/G

Catalytic performance

Reduction of P-NP to P-AP with an excess amount of $NaBH_4$ was selected as an acceptable model reaction to evaluate the catalytic activity of the as-synthesized catalysts. When $NaBH_4$ is added into P-NP solution, absorption peak of p-nitrophenolate ion can be observed at 400 nm [34]. In the presence of the catalyst, the disappearance of the peak of the *p*-nitrophenolate ions is accompanied by a gradual increase of the absorption peak at 300 nm, which corresponds to the formation of P-AP (Fig. 5a) [35].

However, while the reduction reaction did not proceed without any addition of catalysts, the catalytic reaction was quickly started after the addition of a small

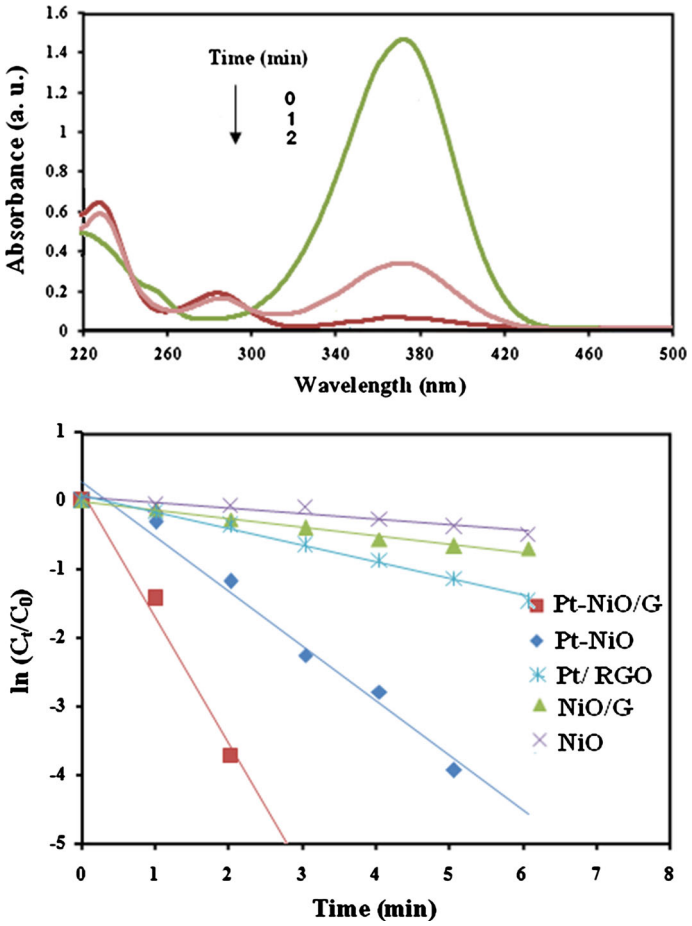

Fig. 5 **a** Time-dependent UV–Vis absorption spectra of P-NP reduction in the presence of the Pt–NiO/G catalyst. **b** The plot of ln (C_t/C_0) versus time of reduction with various catalysts

amount of catalyst. At a high initial concentration of $NaBH_4$, the reaction could be considered to follow a pseudo-first-order kinetic. In order to investigate the kinetics of the catalytic reaction, the plot of ln(C_t/C_0) versus t is shown in Fig. 5b, where C_0 and C_t demonstrate the concentration of P-NP at ithe nitial time and t min after the reaction, respectively. The apparent rate constant (k_{app}) of the P-NP reduction over the samples are given in Fig. 6a. The turnover frequency (TOF) is an important parameter for comparing catalyst efficiency. TOF can be obtained by dividing the number of the substrate molecules which can be converted to products from 1 g of the catalyst by the reaction time. The TOF values of the P-NP reduction by the prepared catalysts are demonstrated in Fig. 6a. Catalytic activity of the as-prepared catalyst and other Pt-based nanocatalysts for the reduction of P-NP were compared and are given in Table 1.

(a)

Sample	k_{app} (min^{-1})	TOF × 10^{20} (Molecule g^{-1} min^{-1})
NiO	0.082	0.0258
NiO/G	0.124	0.0564
Pt/RGO	0.244	0.0645
Pt-NiO	0.892	0.3613
Pt-NiO/G	2.034	0.9033

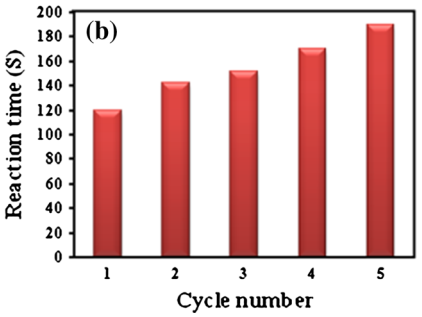

Fig. 6 Apparent rate constant (k_{app}) for NiO, NiO/G, Pt–NiO and Pt–NiO/G (**a**) and the reusability of Pt–NiO/G as catalyst for reduction of P-NP (**b**)

Table 1 Comparison of the activity of various Pt-based catalysts for catalytic P-NP reduction

Catalyst	k_{app} (min^{-1})	TOF × 10^{20} (molecule g^{-1} min^{-1})	References
Pt–NiO/G	2.034	0.9033	This work
Pt–Ni/RGO	0.3700	6.654	[36]
RGO/Pt–Ni	0.0672	0.576	[37]
Fe_3O_4@C–Pt–Pd	1.212	_	[38]
Fe_3O_4@PDA–Pt	0.138	_	[39]
Graphene/SnO_2/Pt	0.88	_	[40]

As can be seen from the rate constants, the addition of Pt significantly promotes the reduction rate and indicates that the introduction of this metal plays an important role in improving the catalytic activity. The Pt–NiO/G composite shows about 24.8 times higher k_{app} than the NiO nanocatalyst, and this enhanced catalytic efficiency can be assigned to the synergistic effect between the NiO and Pt metals.The superior catalytic activity of Pt–NiO/G can be because the presence of Pt induces substantial changes in the surface structure and enhances the adsorption properties. More importantly, the highly dispersed catalyst on the graphene also plays a significant role in improving the catalytic performance, which is obvious from the higher catalytic activity of Pt–NiO/G compared with Pt–NiO.

In order to examine the stability of Pt–NiO/G, which is an important issue for any acceptable catalyst, we performed five successive reduction reactions over the same catalyst which was recovered and washed after each reaction. The reduction reaction time for consecutive cycles is shown in Fig. 6b. The results indicate that the reduction reaction was completed inat 190 s for the fifth cycle. However, a decrease in catalytic performance is seen when metal oxides are used as the catalyst for the reduction of P-NP and therefore additional work is needed to solve this problem.

In addition, the effect of different amounts of catalyst on the catalytic activity was explored. When 2 mg of catalyst was applied, the reduction was completed

before 20 s, while when the amount of catalyst was decreased to 1 and 0.5 mg, the time of reaction increased to 2 and 4.5 min, respectively. These results further illustrate the role of the catalyst in the reduction reaction.

As has been mentioned, for the efficient progress of the reaction of P-NP by $NaBH_4$ a catalyst is required. The mechanism of the reduction reaction can be explained by the Langmuir–Hinshelwood or Eley–Rideal models in heterogeneous catalytic systems. In the first stage of the Langmuir–Hinshelwood mechanism, the *p*-nitrophenolate ion and BH_4^- are chemically adsorbed on the surface of the catalyst and then interfacial electron transfer is initiated [2]. In the case of the Eley–Rideal model, only BH_4^- is adsorbed by the surface of the catalyst generating hydrogen atoms, then these adsorbed hydrogen atoms are taken up by *p*-nitrophenolate in the solution upon collision. It is clear that the surface area of the catalyst affects its catalytic activity in every mechanism. The graphene surface supplies a great number of active sites and plays an important role in improving the catalytic activity. The rate constant dependence on the concentration of $NaBH_4$ and P-NP can indicate a valid mechanism for the reduction reaction. The increase in the concentration of P-NP cause an increase in the rate of the reaction in the Eley–Rideal mechanism, and causes a decrease in the rate of the reaction in the Langmuir–Hinshelwood mechanism.

Figure 7 indicates the relationship between the apparent rate constant and changes in the concentration of BH_4^- and P-NP. The rate constant was decreased with the increase in the concentration of P-NP. Also, the nonlinear dependence of the apparent rate constant values with variation in BH_4^- and P-NP concentrations suggests the competitive adsorption of the reactant and the substrate on the surface of the nanocatalyst [41]. These results suggest that the mechanism of the reduction reaction is the Langmuir–Hinshelwood mechanism. According to this model, the most important step is the reduction of the adsorbed *p*-nitrophenolate ions, because the adsorption of BH_4^- and *p*-nitrophenolate ions on the surface of the catalyst is known to be a rapid and reversible process. Hydrogen atoms transfer to the surface of the catalyst from the adsorbed BH_4^- and are then taken up by the *p*-nitrophenolate ions; this process has been termed as the rate-determining step [42]. It is acceptable that BH_4^- and *p*-nitrophenolate ions are adsorbed on the surface of Pt–NiO/G. A plausible explanation of the enhanced catalytic activity of Pt-modified

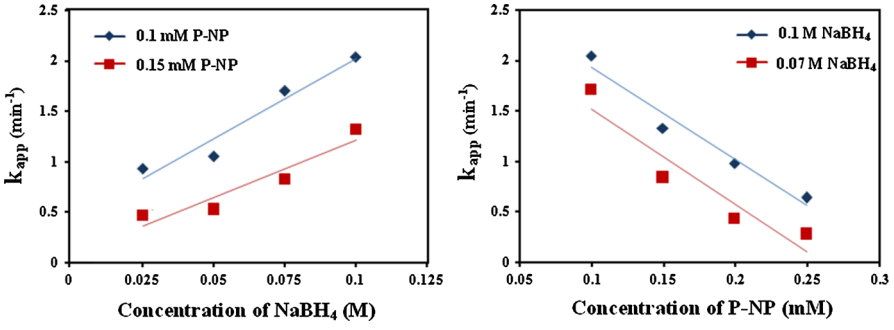

Fig. 7 Effect of $NaBH_4$ and P-NP concentration on apparent rate constant

NiO can be the synergistic effect between Pt and NiO. The hydrogen atoms formed from BH_4^- produce H^+ and e^- to participate in the reduction of P-NP. Due to the work functions of Pt and NiO, electrons tend to transfer to NiO from Pt, and therefore form a depleted region in the Pt/NiO interface, which ends up with an electron-enriched area [43]. The abundant electrons promote the uptake of electrons by the P-NP molecules and accelerate the reduction of P-NP into the P-AP products. The following equations represent the main electron transformation steps involved in the catalytic reduction:

$$\mathrm{Pt} + \mathrm{BH_4^-} \rightarrow \mathrm{Pt}(\mathrm{e^-}, \mathrm{H}) \tag{1}$$

$$\mathrm{NiO} + \mathrm{P-NP} \xrightarrow{\text{absorb}} \mathrm{NiO-P-NP} \tag{2}$$

$$\mathrm{NiO-P-NP} + \mathrm{Pt}(\mathrm{e^-}, \mathrm{H}) \rightarrow\rightarrow\rightarrow \mathrm{Pt} + \mathrm{NiO-P-AP} + \mathrm{H_2O} \tag{3}$$

$$\mathrm{NiO-P-AP} + \xrightarrow{\text{desorb}} \mathrm{NiO} + \mathrm{P-AP} \tag{4}$$

Conclusion

In summary, a Pt–NiO–Al_2O_3/G nanocomposite was prepared by the calcination of graphene supported layered double hydroxide precursors. When employed as the catalyst for the reduction of P-NP in the presence of $NaBH_4$, Pt–NiO/G exhibited much higher catalytic activity than that of NiO/G derived from graphene-supported layered double hydroxide. The enhanced catalytic capability of Pt–NiO/G was mainly attributed to the synergistic effect between Pt and NiO. However, it was proved that the graphene surface supplied a great number of active sites and had an important role in improving the catalytic activity. In addition, a pseudo-first-order kinetic was confirmed for the reduction of P-NP in the presence of Pt-NiO/G, and the Langmuir–Hinshelwood model was suggested for the reduction reaction.

References

1. K.B. Narayanan, N. Sakthivel, J. Hazard. Mater. **198**, 519 (2011)
2. T. Lin, J. Wang, L. Guo, F. Fu, J. Phys. Chem. C **119**, 13658 (2015)
3. R. Krishna, D.M. Fernandes, J. Ventura, C. Freire, E. Titus, Int. J. Hydrog. Energy **41**, 11608 (2016)
4. B.K. Barman, K.K. Nanda, Dalton Trans. **44**, 4215 (2015)
5. Y.C. Chang, D.H. Chen, J. Hazard. Mater. **156**, 664 (2009)
6. Y. Liu, Z. Fang, L. Kuai, B. Geng, Nanoscale **6**, 9791 (2014)
7. H. Yang, W. Vogel, C. Lamy, N. Alonso-Vante, J. Phys. Chem. B **108**, 11024 (2004)
8. S. Senapati, S.K. Srivastava, S.B. Singh, H.N. Mishra, J. Mater. Chem. **22**, 6899 (2012)
9. Y. Imura, K. Tsujimoto, C. Morita, T. Kawai, Langmuir **30**, 5026 (2014)
10. Z. Dong, X. Le, C. Dong, W. Zhang, X. Li, J. Ma, Appl. Catal. B **162**, 372 (2015)
11. O.A. Zelekew, D.-H. Kuo, Phys. Chem. Chem. Phys. **18**, 4405 (2016)
12. C. Huang, W. Ye, Q. Liu, X. Qiu, ACS Appl. Mater. Interfaces **6**, 14469 (2014)
13. B.M. Mogudi, P. Ncube, R. Miejboom, Appl. Catal. B **198**, 74 (2016)

14. J.H. Lee, S.K. Hong, W.B. Ko, J. Ind. Eng. Chem. **16**, 564 (2010)
15. A.K. Sasmal, S. Dutta, T. Pal, Dalton Trans **45**, 3139 (2016)
16. J. Zhao, G. Yu, K. Xin, L. Li, T. Fu, Y. Cui, H. Liu, N. Xue, L. Peng, W. Ding, Appl. Catal. A **482**, 294 (2014)
17. Y.N. Liang, Y. Li, C. Ang, Y. Shen, D. Chi, X. Hu, ACS Appl. Mater. Interfaces **6**, 12406 (2014)
18. L. He, Y. Huang, A. Wang, Y. Liu, X. Liu, X. Chen, J.J. Delgado, X. Wang, T. Zhang, J. Catal. **298**, 1 (2013)
19. Y. Gu, Z. Lu, Z. Chang, J. Liu, X. Lei, Y. Li, X. Sun, J. Mater. Chem. A **1**, 10655 (2013)
20. S. Pausova, J. Krysa, J. Jirkovsky, C. Forano, G. Mailhot, V. Prevot, Appl. Catal. B **170**, 25 (2015)
21. S. Xia, L. Zhang, X. Zhou, M. Shao, G. Pan, Z. Ni, Appl. Catal. B **176**, 266 (2015)
22. R. Xie, G. Fan, Q. Ma, L. Yang, F. Li, J. Mater. Chem. A **2**, 7880 (2014)
23. M. Lan, G. Fan, L. Yang, F. Li, Ind. Eng. Chem. Res. **53**, 12943 (2014)
24. B. Solsona, P. Concepción, J.M. López Nieto, A. Dejoz, J.A. Cecilia, S. Agouram, M.D. Soriano, V. Torres, J. Jiménez, E.R. Castellón, Catal. Sci. Technol. **6**, 3419 (2016)
25. W.X. Chen, J.S. Yu, W. Hu, Z.L. Chen, H. Memon, G.L. Chen, RSC Adv. **6**, 67827 (2016)
26. T.R. Mandlimath, B. Gopal, J. Mol. Catal. A Chem. **350**, 9 (2011)
27. Z. Liang, R. Huo, Y.X. Yin, F. Zhang, S. Xu, Y.G. Guo, Electrochim. Acta **108**, 429 (2013)
28. C. Qi, J.C. Amphlett, B.A. Peppley, Appl. Catal. A **302**, 237 (2006)
29. M.-Q. Yang, Y.-J. Xu, J. Phys. Chem. C **117**, 21724 (2013)
30. F. Zhang, Y. Song, S. Song, R. Zhang, W. Hou, ACS Appl. Mater. Interfaces **7**, 7251 (2015)
31. Y. Ding, Y. Wang, L. Su, H. Zhang, Y. Lei, J. Mater. Chem. **20**, 9918 (2010)
32. S. Wu, K.S. Hui, K.N. Hui, J. Phys. Chem. C **119**, 23358 (2015)
33. L. Wang, X. Lu, C. Wen, Y. Xie, L. Miao, S. Chen, H. Li, P. Li, Y. Song, J. Mater. Chem. A **3**, 608 (2015)
34. W. Gu, X. Deng, X. Jia, J. Li, E. Wang, J. Mater. Chem. A **3**, 8793 (2015)
35. Z. Jiang, D. Jiang, A.M.S. Hossain, K. Qian, J. Xie, Phys. Chem. Chem. Phys. **17**, 2550 (2015)
36. F. Zhao, W. Kong, Z. Hu, J. Liu, Y. Zhao, B. Zhang, RSC Adv. **6**, 79028 (2016)
37. P.K. Sahoo, B. Panigrahy, D. Bahadur, RSC Adv. **4**, 48563 (2014)
38. P. Zhang, R. Li, Y. Huang, Q. Chen, A.C.S. Appl, Mater. Interfaces **6**, 2671 (2014)
39. S.-W. Bian, S. Liu, L. Chang, J. Mater. Sci. **51**, 3643 (2016)
40. C. Zhu, P. Wang, L. Wang, L. Han, S. Dong, Nanoscale **3**, 4376 (2011)
41. N.C. Antonels, R. Meijboom, Langmuir **29**, 13433 (2013)
42. S. Wunder, F. Polzer, Y. Lu, Y. Mei, M. Ballauff, J. Phys. Chem. C **114**, 8814 (2010)
43. J. Fu, C. Zhao, J. Zhang, Y. Peng, E. Xie, ACS Appl. Mater. Interfaces **5**, 7410 (2013)